Shape phase transitions in odd − A Zr isotopes

Nomura, K.; Nikšić, T.; Vretenar, D.

Shape phase transitions in odd-*A* Zr isotopes

K. Nomura,* T. Nikšić, and D. Vretenar
Department of Physics, Faculty of Science, University of Zagreb, HR-10000, Croatia

(Received 30 June 2020; accepted 27 August 2020; published 10 September 2020)

Spectroscopic properties that characterize shape-phase transitions in neutron-rich odd-*A* Zr isotopes are investigated using the framework of nuclear density-functional theory and particle-core coupling. The interacting-boson Hamiltonian of the even-even core nuclei, and the single-particle energies and occupation probabilities of the unpaired neutron, are completely determined by deformation constrained self-consistent mean-field calculations based on the relativistic Hartree-Bogoliubov model with a choice of a universal energy density functional and pairing interaction. The triaxial (β, γ) deformation energy surfaces for even-even $^{94-102}$Zr indicate the occurrence of a transition from triaxial or γ soft (^{94,96}Zr) to prolate (^{98}Zr) and triaxial (^{100,102}Zr) shapes. The corresponding low-energy excitation spectra of the odd-*A* Zr isotopes are in very good agreement with recent experimental results. Consistent with the structural evolution of the neighboring even-even Zr nuclei, the state-dependent effective deformations and their fluctuations in the odd-*A* isotopes indicate a pronounced discontinuity around the transitional nucleus ^{99}Zr.

DOI: 10.1103/PhysRevC.102.034315

I. INTRODUCTION

For many years the structure of neutron-rich nuclei with mass number $A \approx 100$ has been a challenging topic for experiments that use radioactive-ion beams. This particular mass region has also attracted considerable attention in theoretical studies due to its rich microscopic structure. The effective interaction between nucleons determines the corresponding shell structure and gives rise to various shapes, quantum (shape) phase transitions [1] and shape coexistence [2]. Since neutron-rich nuclei in this mass region are also involved in the rapid neutron-capture process, an accurate theoretical description of their low-lying structure and transition rates is important for modeling the formation of chemical elements in various astrophysical scenarios. In many cases the low-energy structure is so rich that it provides an ideal testing ground for theoretical models.

Recently a number of experimental and theoretical studies of spectroscopic properties of even-even Zr isotopes have been reported. Most experimental results have suggested the occurrence of shape coexistence in ^{96}Zr [3] and ^{98}Zr [4,5], a quantum phase transition around the neutron number $N \approx 60$ [6,7] and γ-soft and triaxial shapes at ^{100,102}Zr [8]. Theoretical studies have generally confirmed these experimental findings [3,9–12]. In contrast, much less theoretical research has been devoted to shape-phase transitions in odd-*A* Zr nuclei, for which in the last couple of years several measurements of various spectroscopic properties have been reported, e.g., ^{97}Zr [13] and ^{99}Zr [14,15].

A microscopic calculation of spectroscopic properties of odd-mass nuclei is a challenging task, because in odd-*A* systems one has to take explicitly into account both single-particle and collective degrees of freedom [16]. We have developed a theoretical method [17] for computing spectroscopic properties of odd-*A* nuclei, based on the framework of nuclear density-functional theory (DFT) [18–20] and the particle-core coupling scheme [16]. In this approach the even-even core is described with the interacting boson model (IBM) [21], and the particle-core coupling is fashioned using the interacting boson-fermion model (IBFM) [22]. In a first step a set of constrained self-consistent mean-field (SCMF) calculations is performed for each even-even mass nucleus to provide the potential energy surface (PES). By mapping the SCMF energy surface onto the expectation value of the IBM Hamiltonian, the parameters of the interaction terms of the even-even (boson) core Hamiltonian are completely determined. The same SCMF calculations also provide the spherical single-particle energies and occupation probabilities for the odd nucleon, and these quantities are used as input to construct the boson-fermion interactions. Even though a few boson-fermion interaction strengths have to be adjusted to the empirical low-energy spectra for each odd-*A* nucleus, the method has allowed for a systematic, detailed, and computationally efficient description of spectroscopic properties of nuclei with odd nucleon number(s). So far, this method has been applied to a variety of nuclear structure phenomena in odd-mass and odd-odd nuclei, including quantum phase transitions in axially symmetric [23] and γ soft [24] odd-*A* nuclei, octupole correlations in neutron-rich Ba isotopes [25], chiral band structure in the mass $A \approx 130$ [26] region, and β decay [27,28].

The scope of this work is a simultaneous description of quantum phase transitions that are supposed to take place in the even-even and odd-*A* Zr isotopes, using the aforementioned theoretical method. Here we consider the even-even

*knomura@phy.hr

isotopes $^{94-102}$Zr and the neighboring odd-neutron nuclei $^{95-103}$Zr. The underlying SCMF calculations are carried out within the framework of the relativistic Hartree-Bogoliubov method with the density-dependent point-coupling (DD-PC1) [29] energy density functional and a separable pairing force [30]. SCMF calculations based on the DD-PC1 functional have been successfully applied to various static and dynamic properties of finite nuclei, such as the phenomena of quantum phase transitions [23,24,31], triaxial deformations [32,33], octupole correlations [25,31], shape coexistence [34], clustering [35], and fission dynamics [36,37].

The article is organized as follows. In Sec. II the SCMF energy surfaces for the even-even Zr isotopes are discussed. Section III illustrates the procedure to construct the bosonic and particle-core (IBFM) Hamiltonians for the even-even and odd-A Zr isotopes based on the DFT SCMF calculations. In Sec. IV we discuss spectroscopic properties of even-even and odd-A Zr isotopes in comparison to available data, including low-energy excitation spectra and electromagnetic transition rates, as well as possible signatures of quantum phase transitions (Sec. V). Section VI contains a brief summary of the principal results.

II. SELF-CONSISTENT MEAN-FIELD ENERGY SURFACES FOR EVEN-EVEN ZR ISOTOPES

The first step of the analysis is a set of constrained SCMF calculations of potential energy surfaces for the even-even core nuclei, performed using the relativistic Hartree-Bogoliubov method [19] with the density-dependent point coupling (DD-PC1) [29] functional for the particle-hole channel, and a separable pairing force of finite range [30] in the particle-particle channel. The constraints imposed in the SCMF calculations are the mass quadrupole moments, which are represented by the dimensionless quadrupole deformation parameters β and γ [16].

In Fig. 1 we display the SCMF (β, γ) energy surfaces for $^{94-102}$Zr. Several remarkable features appear already at the mean-field level. The nucleus ^{94}Zr exhibits a pronounced triaxial minimum at $\gamma \approx 40^\circ$, even though it is located near the neutron shell closure at $N = 50$. For ^{96}Zr, the potential becomes more γ soft, and essentially two shallow minima appear, one on the prolate and the other on the oblate side. A prolate local minimum between $\beta = 0.4$ and 0.5 is also visible. The structure appears to change significantly at ^{98}Zr: While the surface is still rather flat in the γ direction for the interval $0.2 \leqslant \beta \leqslant 0.3$, a pronounced prolate minimum develops at around $\beta = 0.5$ and becomes the equilibrium configuration. This prolate minimum develops even further for ^{100}Zr but, compared to ^{98}Zr, the surface again becomes softer in γ. Finally, in ^{102}Zr a triaxial global minimum is found at $\gamma \approx 15^\circ$. Those γ-soft and triaxial shapes obtained for ^{100,102}Zr are compatible with recent experimental results [8].

It might be useful to note some predictions obtained using different EDFs. In particular, results of Hartree-Fock-Bogoliubov calculations based on the Gogny-D1S [38] EDF are available [39]. The Gogny-HFB calculations predict an almost spherical shape for ^{94}Zr and a weakly deformed oblate shape for ^{96}Zr. They also determine a coexistence of oblate (at $\beta \approx 0.2$) and prolate (at $\beta \approx 0.5$) minima in ^{96}Zr consistent with the result of the present work, but in the former case the global minimum is on the oblate side. For the deformed nuclei ^{100,102}Zr, the Gogny-HFB surfaces appear rather similar to the present results. The Gogny-HFB calculation with the D1M EDF [40] has also been reported in Ref. [10]. The D1M energy surfaces are generally softer but not strikingly different from the D1S ones. A noticeable difference between the two Gogny EDFs is that with the D1M EDF an oblate global minimum is obtained for ^{100}Zr.

III. CONSTRUCTION OF THE FERMION-BOSON HAMILTONIAN

To calculate spectroscopic properties of nuclei, the static mean-field method has to be extended to include collective correlations that arise from symmetry restoration and fluctuations around mean-field minima [41]. In the present work collective correlations are taken into account by mapping the SCMF solutions onto the corresponding interacting-boson systems [42]. The coupling of the odd nucleon to the even-even core is described within the neutron-proton interacting boson-fermion model (denoted hereafter as IBFM-2).

The complete IBFM-2 Hamiltonian consists of the neutron-proton IBM (IBM-2) [43] Hamiltonian $\hat{H}_B$ for the even-even core nucleus, the single-neutron or proton Hamiltonian $\hat{H}_F^\rho (\rho = \nu/\pi)$, and the Hamiltonian that represents the coupling between the odd neutron/proton and the boson core $\hat{H}_{\rm BF}^\rho$:

$$\hat{H} = \hat{H}_B + \hat{H}_F^\nu + \hat{H}_F^\pi + \hat{H}_{\rm BF}^\nu + H_{\rm BF}^\pi. \quad (1)$$

For the IBM-2 Hamiltonian we employ the following form, which has been shown [10] to provide a good description of spectroscopic data in this mass regions:

$$\hat{H}_B = \epsilon\left(\hat{n}_{d_\nu} + \hat{n}_{d_\pi}\right) + \kappa \hat{Q}\cdot\hat{Q} + \kappa' \sum_{\rho'\neq\rho} \hat{T}_{\rho\rho\rho'} + \kappa'' \hat{L}\cdot\hat{L}, \quad (2)$$

where the first term $\hat{n}_d = \hat{n}_{d_\nu} + \hat{n}_{d_\pi}$, with $\hat{n}_{d_\rho} = d_\rho^\dagger \cdot \tilde{d}_\rho$ $(\rho = \nu, \pi)$, represents the d-boson number operator, and $\hat{Q} = \hat{Q}_\nu + \hat{Q}_\pi$ is the quadrupole operator with $\hat{Q}_\rho = s_\rho^\dagger \tilde{d}_\rho + d_\rho^\dagger \tilde{s}_\rho + \chi_\rho [d_\rho^\dagger \times \tilde{d}_\rho]^{(2)}$. The third term is a specific three-body boson interaction [32] with $\hat{T}_{\rho\rho\rho'} = \sum_L [d_\rho^\dagger \times d_\rho^\dagger \times d_{\rho'}^\dagger]^{(L)} \cdot [\tilde{d}_{\rho'} \times \tilde{d}_\rho \times \tilde{d}_\rho]^{(L)}$, where L denotes the total angular momentum of the boson system. As in Refs. [10,32], we consider only the $L = 3$ terms, since they play a dominant role in producing minima at $\gamma \approx 30^\circ$. The last term in Eq. (2) is the rotational Hamiltonian with the angular momentum operator $\hat{L} = \hat{L}_\nu + \hat{L}_\pi = \sqrt{10} \sum_{\rho=\nu,\pi} [d_\rho^+ \times \tilde{d}_\rho]^{(1)}$.

The single-nucleon Hamiltonian in Eq. (1) reads:

$$\hat{H}_F^\rho = -\sum_{j_\rho} \epsilon_{j_\rho} \sqrt{2j_\rho + 1} \left(a_{j_\rho}^\dagger \times \tilde{a}_{j_\rho}\right)^{(0)} \quad (3)$$

with ϵ_{j_ρ} the single-particle energy of the spherical orbital j_ρ. For the boson-fermion interaction $\hat{H}_{\rm BF}^\rho$, we employ the commonly used form [22]:

$$\hat{H}_{\rm BF}^\rho = \Gamma_\rho \hat{Q}_{\rho'} \cdot \hat{q}_\rho + \Lambda_\rho \hat{V}_{\rho'\rho} + A_\rho \hat{n}_{d_\rho} \hat{n}_\rho, \quad (4)$$

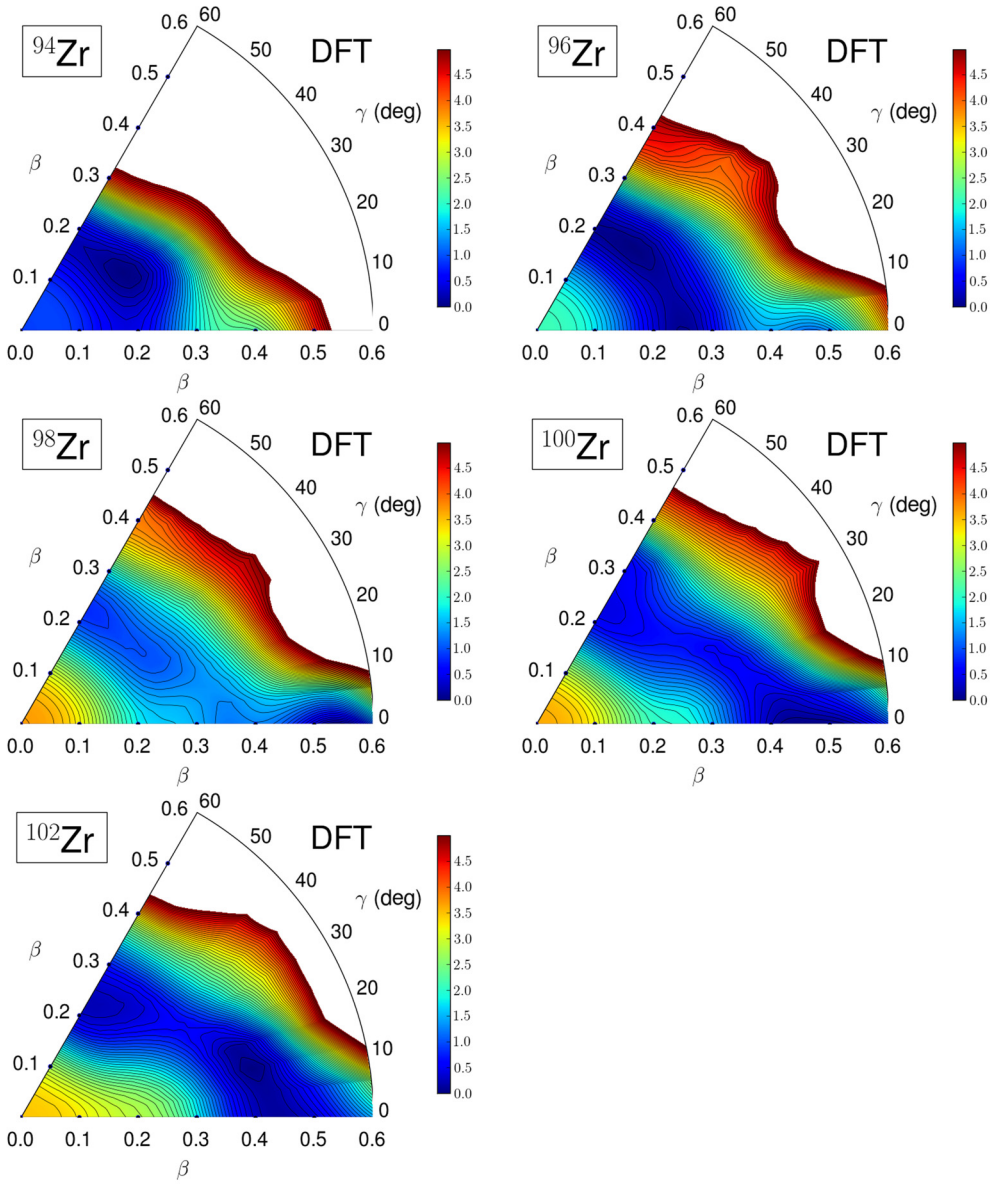

FIG. 1. SCMF (β, γ) deformation energy surfaces (in MeV) for the even-even nuclei $^{94-102}$Zr, obtained from constrained relativistic Hartree-Bogoliubov calculations using the DD-PC1 functional [29] and a separable pairing force [30]. The total SCMF energies are plotted to 5 MeV with respect to the global minimum. The energy difference between neighboring contours is 100 keV.

where $\rho' \neq \rho$. The first, second, and third terms in the equation above are the quadrupole dynamical, exchange, and monopole interactions, respectively. It is assumed that both the dynamical and exchange terms are dominated by the interaction between unlike particles (i.e., between the odd neutron and the proton bosons or between the odd proton and the neutron bosons), and that, for the monopole term, the interaction between like particles (i.e., between the odd neutron and the neutron bosons or between the odd proton and the proton bosons) plays a dominant role [22]. The fermionic quadrupole operator $\hat{q}_\rho$ reads:

$$\hat{q}_\rho = \sum_{j_\rho j'_\rho} \gamma_{j_\rho j'_\rho} \left(a^\dagger_{j_\rho} \times \tilde{a}_{j'_\rho}\right)^{(2)}, \tag{5}$$

where $\gamma_{j_\rho j'_\rho} = (u_{j_\rho} u_{j'_\rho} - v_{j_\rho} v_{j'_\rho}) Q_{j_\rho j'_\rho}$ and $Q_{j_\rho j'_\rho} = \langle l \tfrac{1}{2} j_\rho || Y^{(2)} || l' \tfrac{1}{2} j'_\rho \rangle$. The exchange term $\hat{V}_{\rho'\rho}$ in Eq. (4) can be written as:

$$\hat{V}_{\rho'\rho} = -(s^\dagger_{\rho'} \tilde{d}_{\rho'})^{(2)} \left\{ \sum_{j_\rho j'_\rho j''_\rho} \sqrt{\frac{10}{N_\rho (2j_\rho + 1)}} \beta_{j_\rho j'_\rho} \beta_{j''_\rho j_\rho} \right.$$
$$\left. : \left[\left(d^\dagger_\rho \times \tilde{a}_{j''_\rho}\right)^{(j_\rho)} \times \left(a^\dagger_{j'_\rho} \times \tilde{s}_\rho\right)^{(j'_\rho)} \right]^{(2)} : \right\} + (\text{H.c.}), \tag{6}$$

with $\beta_{j_\rho j'_\rho} = (u_{j_\rho} v_{j'_\rho} + v_{j_\rho} u_{j'_\rho}) Q_{j_\rho j'_\rho}$.

In this work, the nearest doubly magic nucleus ^{100}Sn is taken as the boson vacuum. The neutron boson number N_ν

is then equal to the number of valence neutron pairs, that is, $N_\nu = 2, 3, 4, 5$, and 6 for the even-even nuclei from ^{94}Zr to ^{102}Zr, respectively. The proton boson number $N_\pi = 5$ is fixed and equals the number of proton hole pairs. We note that in several previous IBM calculations [11,12] the proton $Z = 40$ subshell was taken as the inert core for the proton bosons in Zr isotopes. In those studies two independent IBM Hamiltonians, one for the regular configuration with the proton boson number $N_\pi = 0$ and the other for the intruder configuration with $N_\pi = 2$ associated with the proton two-particle-two-hole excitation across the shell $Z = 40$, are considered and allowed to mix in order to account for shape coexistence [44]. It is, however, beyond the scope of the present work to include intruder configurations and the corresponding configuration mixing. The $Z = 40$ subshell could also be used here as the proton inert core but, from a practical point of view, the IBM model space with the proton boson number $N_\pi = 0$ plus the neutron boson number $2 \leqslant N_\nu \leqslant 6$ would be far too small for a quantitative description of collective physical observables. In addition, for $N_\pi = 0$ the dynamical and exchange odd neutron-boson interactions in Eq. (4) do not contribute to odd-A Zr isotopes.

The structure of the odd-A Zr nuclei is described as a system with a single (unpaired) neutron coupled to the even-even boson-core with mass number $A - 1$. For the fermion valence space, we consider the full neutron major shell $N = 50$–82, i.e., the $3s_{1/2}$, $2d_{3/2}$, $2d_{5/2}$, and $1g_{7/2}$ spherical orbitals for positive-parity states, and the unique-parity $1h_{11/2}$ orbital for negative-parity states.

The first step in the construction of the particle-boson Hamiltonian Eq. (1) is to specify the strength parameters for the IBM-2 Hamiltonian $\hat{H}_B$. The parameters ϵ, κ, χ_ν, χ_π, and κ' are completely determined by mapping the SCMF energy surface in the vicinity of the global minimum onto the expectation value of the IBM-2 Hamiltonian in the boson coherent state [42], i.e., $E_{\rm SCMF}(\beta, \gamma) \approx E_{\rm IBM}(\beta, \gamma)$. Only the strength parameter κ'' of the $\hat{L} \cdot L$ term has been determined separately, in such a way [45] that the cranking moment of inertia in the bosonic intrinsic state should reproduce the one computed by the SCMF within the relevant range of $|\beta| \leqslant 0.6$. The mapped IBM-2 energy surfaces, depicted in Fig. 2, reproduce the corresponding SCMF surfaces. In addition, we list in Table I the strength parameters for the boson-core Hamiltonian. The positive sign of the parameter κ' for ^{94}Zr leads to a triaxial minimum, while the opposite sign obtained for all the other nuclei produces the two minima on the energy surface corresponding to prolate and oblate shapes. A previous IBM calculation of Ref. [46] has also used the three-body term to produce the two minima. However, the three-body term has a rather minor effect on the excitation spectra except for the γ band [32], and its contribution is shown to be even weaker when the strength parameter κ' has a negative sign. It is, therefore, expected that the contribution of this term to the low-lying states in the odd-A systems, at least near the yrast line, is also small. In addition, since the current IBFM code is limited to two-body boson interactions, in the following calculations for the odd-A Zr isotopes the three-body boson terms are not included.

The Hamiltonians for the single neutron $\hat{H}_F^\nu$ and the boson-fermion interaction $\hat{H}_{\rm BF}^\nu$ are determined by using the method developed in Ref. [17]. The spherical single-particle energies ϵ_j and occupation probabilities v_j^2 of the odd-neutron orbital j are provided by the same constrained SCMF calculations. In the following, since we consider for the fermionic degree of freedom only an odd neutron, the terms $\hat{H}_F^\pi$ and $\hat{H}_{\rm BF}^\pi$ in Eq. (1), as well as the subscript ρ in j_ρ's are omitted. The strength parameters for the boson-fermion interaction $\hat{H}_{\rm BF}$, denoted by Γ^{sdg}, Λ^{sdg}, and A^{sdg} (Γ^h, Λ^h, and A^h) for positive (negative) parity, are treated as the only free parameters and are determined separately for each parity to reproduce the experimental low-lying excitation spectra. The criteria for fitting these parameters are that the spin of the ground state (i.e., the lowest-energy state for each parity) should be reproduced, as well as the excitation energies of few lowest yrast states to a reasonable accuracy. Of course, the overall systematics of the lowest bands, i.e., the energy level spacing within the bands and the observed $\Delta I = 1$ or 2 systematics, should also be reproduced. Transition strengths are not taken into account in the fitting procedure.

The adopted ϵ_j and v_j^2 for each orbital, and the boson-fermion interaction strengths are shown in Tables II and III, respectively. As the strength parameters are adjusted for each odd-A nucleus, they should reflect the corresponding difference in structure between neighboring isotopes. For instance, there are significant differences in these parameters between ^{95}Zr and ^{97}Zr both for the sdg (positive-parity) and $h_{11/2}$ (negative-parity) configurations. In addition, one may notice in Table III that unusually large values of the exchange interaction strengths are chosen for the $1h_{11/2}$ configuration in $^{97-103}$Zr. In many IBFM calculations the typical value of this parameter is a few MeVs. In the present case the large values arise because the occupation probabilities for the $1h_{11/2}$ orbital obtained from the SCMF calculation are very small, e.g., $v^2_{h_{11/2}} = 0.020$ for ^{97}Zr (see Table II), and, consequently, the factor $\beta^2_{jj} \propto u_j^2 v_j^2$ in Eq. (6) is also small. In order to account for the small v_j^2 values, a large strength for the exchange term Λ is required specifically for the $1h_{11/2}$ configuration. In fact, the resulting constant $\Lambda_{jj} \equiv \beta^2_{jj}\sqrt{10/N_\nu(2j+1)}$ takes a realistic value, e.g., for ^{97}Zr, for which the largest Λ^h is obtained, it is approximately $\Lambda_{jj} = -2.2$ MeV. We also note that such large exchange strength parameters of the order $\Lambda \approx 50$ MeV were already considered in some previous studies, e.g., in Ref. [47].

The resulting IBFM-2 Hamiltonian, with the parameters thus determined, is diagonalized to produce excitation energies and transition rates for a given odd-A nucleus.

IV. SPECTROSCOPIC PROPERTIES

A. Excitation spectra of even-even Zr isotopes

The energy spectra of low-lying excited states in the even-even Zr isotopes are depicted in Fig. 3. The transition between different shapes with increasing neutron number is characterized by the rapid decrease of the low-spin levels starting from ^{96}Zr to ^{100}Zr. The fact that the lowest levels for ^{96}Zr are

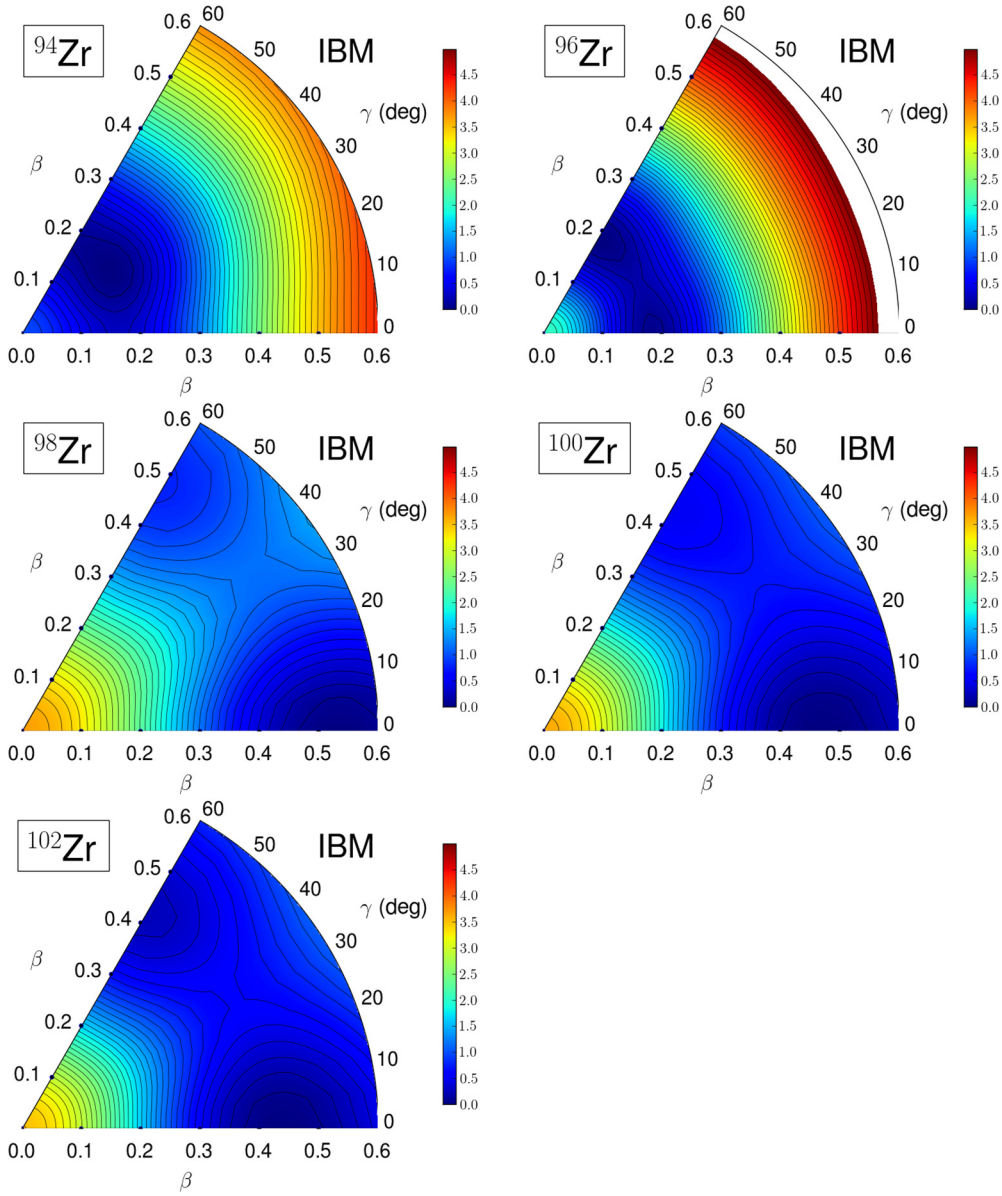

FIG. 2. The bosonic energy surfaces based on the IBM-2 Hamiltonian in Eq. (2), with the parameters determined by the corresponding constrained SCMF calculations.

found at rather high energy when compared to the neighboring isotopes points to the $N = 56$ neutron subshell closure (due to the filling of the $2d_{5/2}$ orbital), and the sudden decreases of the energy levels from $N = 56$ toward $N = 60$ corresponds to the enhancement of collectivity. As shown in Fig. 3, these empirical features are qualitatively reproduced by the present calculation.

TABLE I. Strength parameters of the IBM-2 Hamiltonian $\hat{H}_B$ for the even-even nuclei $^{94-102}$Zr. All the parameters, except the dimensionless χ_ν and χ_π, are in units of MeV.

	ϵ	κ	χ_ν	χ_π	κ'	κ''
^{94}Zr	0.501	−0.075	−0.06	0.21	0.28	0.029
^{96}Zr	0.345	−0.090	−0.35	0.24	−0.12	0.051
^{98}Zr	0.284	−0.073	−0.54	0.11	−0.32	0.032
^{100}Zr	0.036	−0.047	−0.45	0.20	−0.12	0.002
^{102}Zr	0.081	−0.040	−0.52	0.49	−0.10	0.004

One notices, however, that the excitation energies of the second 0^+ state in the nuclei ^{98,100}Zr are predicted far too high with respect to their experimental counterparts. The occurrence of very low-lying excited 0^+ states is often attributed to effects such as shape coexistence related to intruder configurations, and to pairing vibrations, both of which are outside the model space of the present IBM framework. Several recent IBM calculations [10–12] that include the effects of intruder excitations across the proton $Z = 40$ subshell closure and configuration mixing of normal and intruder configurations, reproduced the 0_2^+ excitation energies. A drawback of such

TABLE II. Neutron single-particle energies ϵ_j (in MeV) and occupation probabilities v_j^2 obtained from spherical SCMF calculations for the odd-A nuclei ^{95,97,99,101,103}Zr.

		$3s_{1/2}$	$2d_{3/2}$	$2d_{5/2}$	$1g_{7/2}$	$1h_{11/2}$
^{95}Zr	ϵ_j	−4.322	−3.838	−6.219	−5.199	−0.894
	v_j^2	0.078	0.068	0.484	0.204	0.014
^{97}Zr	ϵ_j	−4.557	−4.038	−6.418	−5.499	−1.149
	v_j^2	0.127	0.099	0.604	0.327	0.020
^{99}Zr	ϵ_j	−4.773	−4.241	−6.614	−5.801	−1.409
	v_j^2	0.188	0.135	0.699	0.462	0.026
^{101}Zr	ϵ_j	−4.970	−4.445	−6.806	−6.099	−1.671
	v_j^2	0.265	0.181	0.777	0.600	0.031
^{103}Zr	ϵ_j	−5.146	−4.643	−6.993	−6.388	−1.929
	v_j^2	0.367	0.245	0.843	0.730	0.036

extended calculations is that, since two independent Hamiltonians associated with different boson numbers need to be introduced [44], the number of model parameters increases significantly. In particular, the extension of this formalism to odd-mass systems, i.e., to the case of an odd nucleon coupled to the configuration-mixing IBM core, becomes exceptionally complex. The current implementation of the IBFM does not perform configuration mixing in the boson space and, therefore, here the calculation for the even-even Zr isotopes is carried out without the inclusion of intruder excitations and configuration mixing.

For ^{94,96}Zr the present calculation predicts a level structure characterized by the energy ratio $E(4_1^+)/E(2_1^+) > 2$. This is at variance with the experimental results, which exhibit a smaller ratio $E(4_1^+)/E(2_1^+) < 2$. The discrepancy could be accounted for by the fact that the employed IBM consists of only collective nucleon pairs of monopole and quadrupole types (i.e., s and d bosons). For the transitional nucleus ^{98}Zr, the 2_1^+ level is particularly low, as in the case of ^{96}Zr. In our calculation the lowest-lying states for ^{98}Zr are mostly based on configurations located close to the prolate global minimum at $\beta \approx 0.5$ on the SCMF energy surface. The resulting IBM spectra are likely to be more rotational-like than observed in experiment. We obtain γ-soft spectra for ^{100,102}Zr, and this result is consistent with the underlying SCMF surfaces, which are indeed soft in the γ degree of freedom.

TABLE III. The adopted values for the boson-fermion strength parameters of the IBFM-2 Hamiltonian $\hat{H}_{\rm BF}$, used for the sdg and $h_{11/2}$ configurations to describe the positive- and negative-parity low-lying states, respectively, of the odd-A nuclei $^{95-103}$Zr. All entries in the table are in the units of MeV.

	Γ^{sdg}	Λ^{sdg}	A^{sdg}	Γ^{h}	Λ^{h}	A^{h}
^{95}Zr	0.1	0.0	0.0	0.4	0.4	0.0
^{97}Zr	0.3	3.6	0.0	0.5	47.0	4.0
^{99}Zr	0.5	1.3	−4.0	0.5	30.0	−3.0
^{101}Zr	0.5	0.66	−0.3	0.1	17.0	−0.0
^{103}Zr	0.2	0.66	0.0	0.2	12.6	0.0

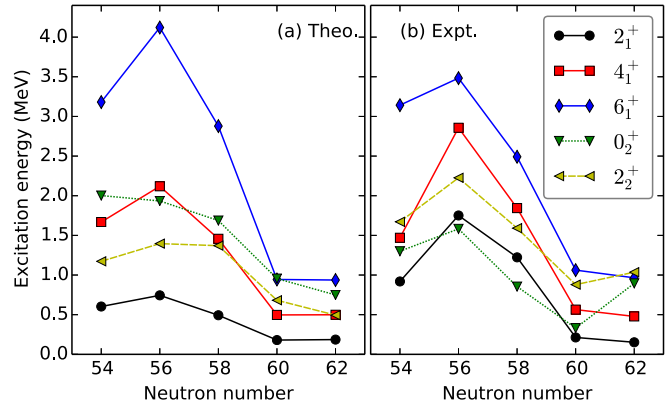

FIG. 3. Low-energy excitation spectra of the even-even isotopes $^{94-102}$Zr, calculated with the IBM-2 Hamiltonian of Eq. (2). The corresponding data, taken from the compilation of the ENSDF database [48], are included for comparison.

B. Excitation spectra of odd-A Zr isotopes

The principal scope of this work are spectroscopic calculations of structural evolution in the odd-A Zr isotopes, and in the following we discuss in much more detail the results for odd-A systems. First, in Fig. 4 we display the systematics of calculated excitation spectra for the low-lying positive- and negative-parity yrast states of the odd-A Zr isotopes, in comparison to available data [13,14,48,49]. The excitation energies of negative-parity states are plotted with respect to the energy of the lowest-lying negative parity state. One notices that the calculated spectra reproduce very nicely the experimental results for both parities, except perhaps for the excitation energy of $3/2^-$ in most of the odd-A Zr.

For both parities the level structure changes significantly between ^{97}Zr and ^{101}Zr. The fact that the experimental spectra are particularly expanded at $N = 57$, that is, the excitation energies of most levels exhibit peaks at $N = 57$, is interpreted as an effect of the neutron $2d_{5/2}$ subshell filling in the corresponding even-even core nucleus ^{96}Zr. The calculated positive-parity states are in better agreement with experiment compared to the negative-parity states, in particular at $N = 57$. This is probably because for the negative parity only the unique-parity $1h_{11/2}$ orbital is considered. For the lighter odd-A Zr isotopes the energy spectra of ^{95,97}Zr appear almost harmonic. In the transitional region at ^{99}Zr many of the yrast levels are lowered in energy, and a more complicated low-lying structure with higher level density emerges. For negative-parity states, in particular, many of the higher-spin levels exhibit a sharp lowering in energy at the neutron number $N = 59$. For the heavier isotopes ^{101,103}Zr, we find a more regular pattern of excitation spectra, characterized by the $\Delta I = 1$ level sequence with increasing angular momentum. As one notices from Figs. 4(c) and 4(d), in most odd-A nuclei the spin of the calculated lowest negative-parity state is at variance with data. This could be due to the calculated occupation number $v^2_{h_{11/2}}$ and the resulting boson-core interaction. However, we also note that the lowest-state spins for the negative-parity states are, in many cases, not firmly established experimentally [48].

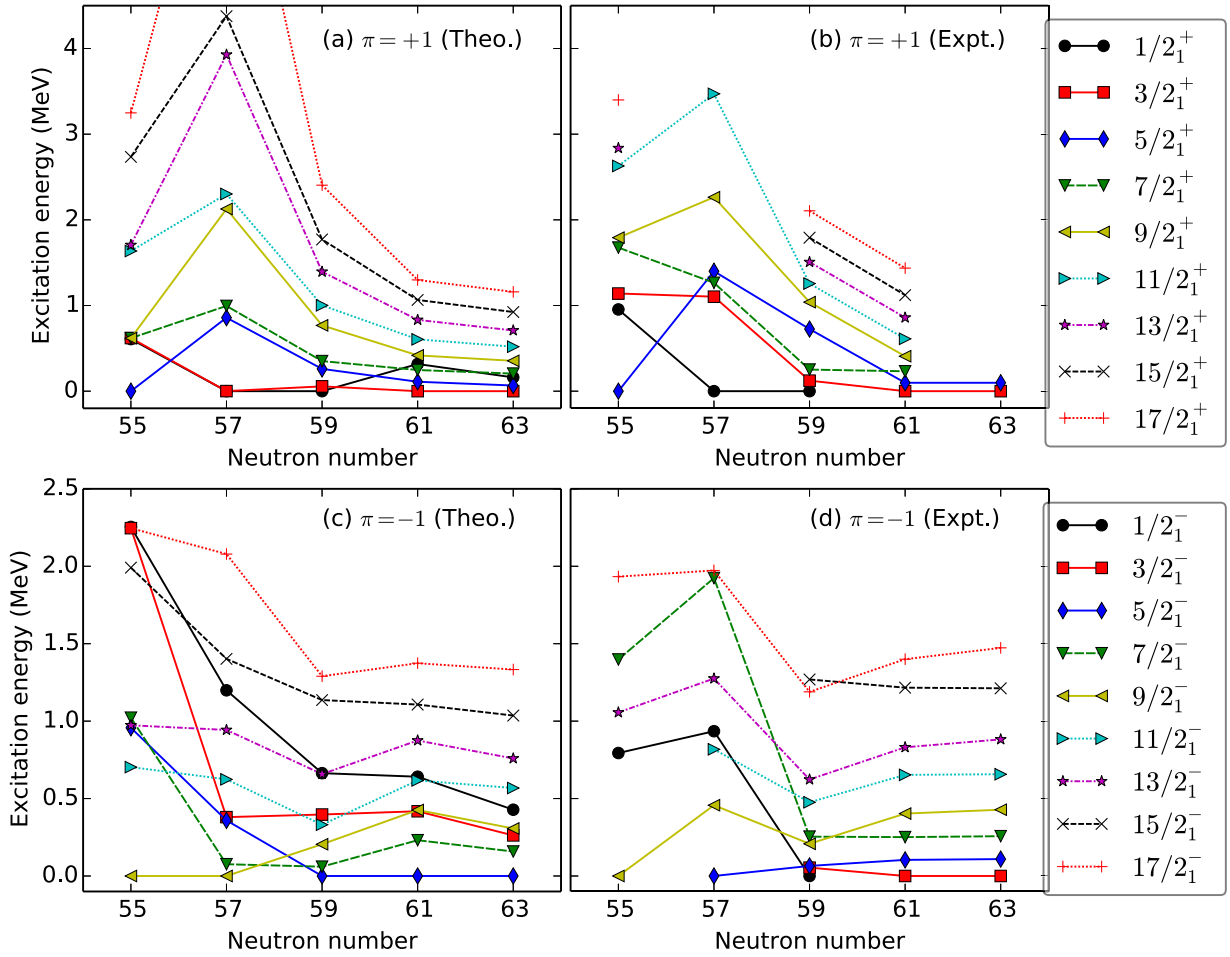

FIG. 4. Excitation spectra for the low-lying positive [(a) and (b)] and negative-parity [(c) and (d)] states of the odd-*A* nuclei $^{95-103}$Zr. The experimental levels are from Refs. [13,14,48,49].

C. Detailed level schemes of selected odd-*A* Zr nuclei

It is interesting to consider in more detail the excitation spectra of individual odd-*A* Zr isotopes in the transitional region. Figures 5–7 display the lowest band structures of both parities in ^{97,99,101}Zr, which are most relevant for the discussion of a shape transition. Included are also the corresponding experimental spectra for comparison. To help with the analysis of the structure of the lowest positive-parity states, in Fig. 8 we plot the the probability amplitudes of the $3s_{1/2}$, $2d_{3/2}$, $2d_{5/2}$, and $1g_{7/2}$ single-particle configurations in the wave functions of the yrast states $1/2_1^+$, $3/2_1^+$, $5/2_1^+$, and $7/2_1^+$.

1. ^{97}Zr

There is no definite band structure established experimentally in ^{97}Zr. As it can be deduced from Fig. 8, it appears that all four single-particle configurations ($3s_{1/2}$, $2d_{3/2}$, $2d_{5/2}$, and $1g_{7/2}$) almost equally contribute to the composition of the wave functions of the lowest-lying positive-parity states. Our calculation predicts two $\Delta I = 2$ positive-parity bands characteristic for the weak-coupling limit, and a $\Delta I = 1$ band with a pronounced doublet structure built on the $1/2_2^+$. At variance with the data, the $3/2_1^+$ state is calculated too low in energy, just a few keV above the $1/2^+$ ground state. For the negative-parity states, the calculation predicts many more levels than observed in experiment so far, and also the $E2$

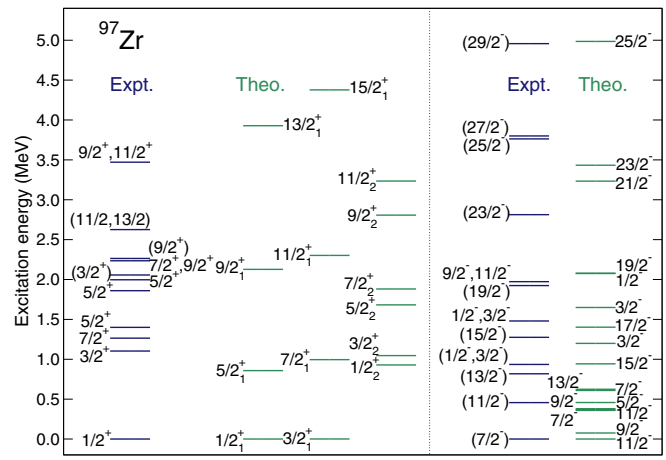

FIG. 5. Comparison between theory and experiment [13,48] for the positive (left) and negative-parity (right) excitation spectrum of ^{97}Zr.

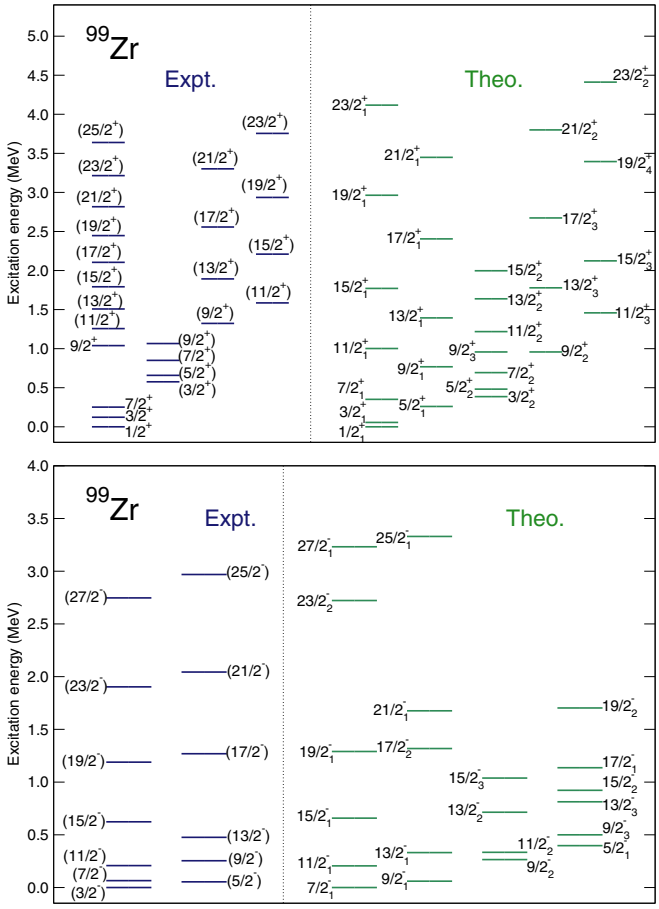

FIG. 6. Band structure of theoretical positive (upper panel) and negative-parity (lower panel) excitation spectra of ^{99}Zr in comparison to the available data [14,48].

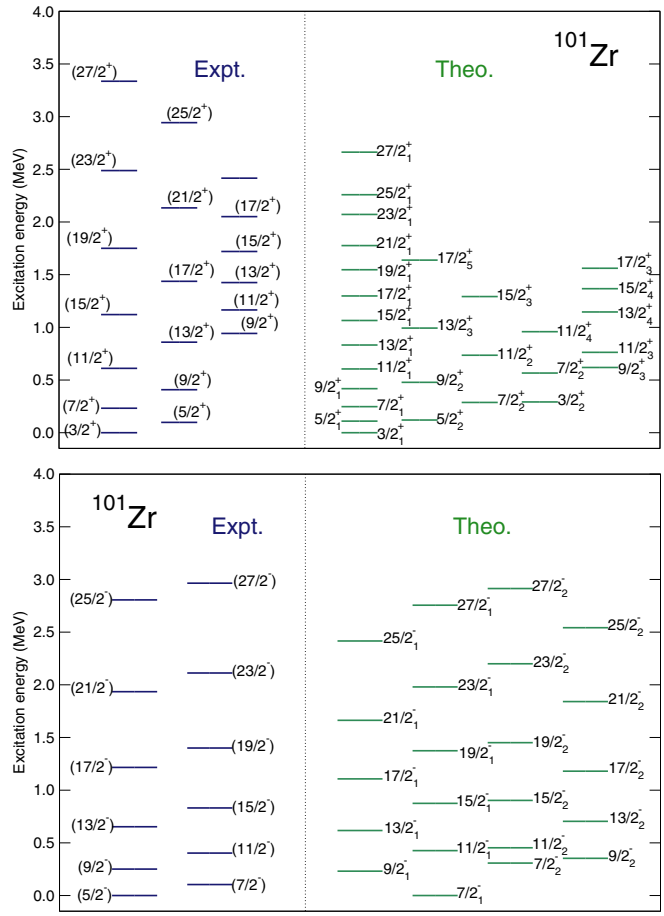

FIG. 7. Same as in the caption to Fig. 6, but for the nucleus ^{101}Zr. The data are from Ref. [48,50].

strengths of these states are strongly fragmented. This makes the assignment of low-lying negative-parity states into bands almost impossible.

2. ^{99}Zr

Unlike ^{97}Zr, several band structures have recently been experimentally identified in the nucleus ^{99}Zr [14,15,48]. Both the experimental and theoretical positive-parity energy spectra in Fig. 6 exhibit strongly coupled $\Delta I = 1$ and weakly coupled $\Delta I = 2$ bands coexisting at low energy. As seen in Fig. 8, the structure of the low-lying low-spin positive-parity yrast states is similar to that of ^{97}Zr: All four single-particle configurations equally contribute to the IBFM-2 wave functions. For instance, in the $1/2^+_1$ ground state the $3s_{1/2}$, $2d_{3/2}$, $2d_{5/2}$, and $1g_{7/2}$ single-particle configurations contribute with probabilities of 21%, 27%, 31%, and 21%, respectively. In contrast, most of the states in the $\Delta I = 1$ band based on the $3/2^+_2$ state, are predominantly (about 80%) composed of the $2d_{5/2}$ single-particle configuration. Another two $\Delta I = 2$ weakly coupled bands built on top of the $9/2^+_2$ and $11/2^+_3$ states are predicted. The main component of these bands is, again, the $2d_{5/2}$ configuration, especially for higher-spin states in the bands. In the lower-spin states close the $9/2^+_2$ and $11/2^+_3$ band heads, the four single-particle configurations are so strongly mixed, that the band assignment for these states according to the systematics of the $E2$ transitions is not very certain.

The experimental negative-parity spectra look much more regular, with only two $\Delta I = 2$ bands extending to high-spin. The calculation reproduces the overall structure of the experimental negative-parity spectra but does not confirm the assigned band heads of the two $\Delta I = 2$.

3. ^{101}Zr

The even-even core for this nucleus (^{100}Zr) is located near the end of the phase transition, and the (β, γ) energy surface exhibits a more extended prolate deformation at large β. In contrast to ^{97,99}Zr, the lowest-lying positive-parity states for ^{101}Zr are predominantly composed of the $1g_{7/2}$ (≈20%) and $2d_{5/2}$ (≈80%) single-particle configurations (see Fig. 8). The excitation spectra for both parities display a more regular band structure compared to ^{97,99}Zr, and the states in each band are connected by strong $E2$ transitions. The calculated yrast band built on the $3/2^+_1$ ground state follows the strong-coupling $\Delta I = 1$ systematics of the $E2$ transitions. The second excited band in experiment, based on the tentatively assigned $9/2^+$ state at 940 keV, could be compared with the predicted strong-coupling $\Delta I = 1$ band built on the $9/2^+_3$ state at 619 keV.

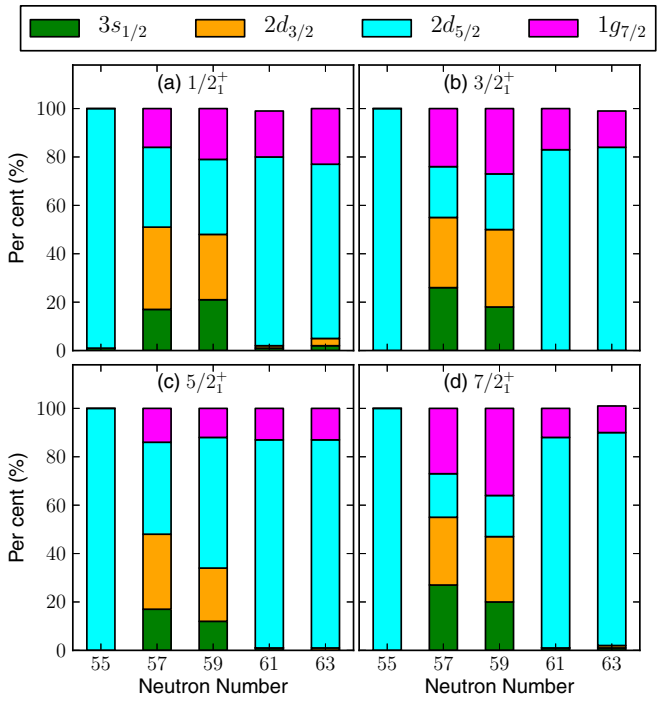

FIG. 8. Probability amplitudes of the $3s_{1/2}$, $2d_{3/2}$, $2d_{5/2}$, and $1g_{7/2}$ single-neutron configurations in the wave functions of the calculated positive-parity yrast states $1/2_1^+$ (a), $3/2_1^+$ (b), $5/2_1^+$ (c), and $7/2_1^+$ (d) in the odd-A isotopes $^{95-103}$Zr.

However, one should keep in mind that this band has been assigned to the state 9/2[404] associated with the proton $1g_{9/2}$ intruder state [50], whereas this state is not included in the configuration space of the present IBFM-2 calculation.

For the negative-parity two $\Delta I = 2$ structures have been empirically identified as yrast bands. Several $\Delta I = 2$ bands are also obtained in the calculation. The lowest two reproduce the excitation energies of the experimental bands but differ in spin by one unit. As mentioned above, this can partly be due to the limited IBFM-2 space that includes only the $1h_{11/2}$ negative-parity orbital. Note, however, that the spin assignment for the experimental states is tentative. Also the theoretical band assignment in this case may not be unique, since several states with the same spin are calculated within a small energy interval and, because of mixing, their $E2$ transitions are weak and fragmented. The band structure for the neighboring nucleus ^{103}Zr is similar to the one obtained for ^{101}Zr but is not discussed here since there are no data available.

D. Electromagnetic properties

There is also limited experimental information about the electromagnetic transition rates for the odd-A Zr isotopes. These properties are readily computed using the eigenstates of the IBFM-2 Hamiltonian. The $E2$ operator $\hat{T}^{(E2)}$ in the IBFM-2 takes the form [22]:

$$\hat{T}^{(E2)} = e_\nu^B \hat{Q}_\nu + e_\pi^B \hat{Q}_\pi - \frac{1}{\sqrt{5}} e^F \sum_{jj'} \gamma_{jj'} (a_j^\dagger \times \tilde{a}_{j'})^{(2)}, \quad (7)$$

where the fixed values for the boson effective charges $e_\nu^B = e_\pi^B = 0.10\ e$b are chosen so that the $B(E2; 2_1^+ \to 0_1^+)$ values for the deformed even-even core nuclei, i.e., ^{100,102}Zr, are reproduced. The neutron effective charge $e^F = 0.5\ e$b is adopted from our earlier calculation [26]. The $M1$ transition operator $\hat{T}^{(M1)}$ reads

$$\hat{T}^{(M1)} = \sqrt{\frac{3}{4\pi}} \left\{ g_\nu^B \hat{L}_\nu^B + g_\pi^B \hat{L}_\pi^F - \frac{1}{\sqrt{3}} \sum_{jj'} (u_j u_{j'} + v_j v_{j'}) \times \langle j' \| g_l^\nu \mathbf{l} + g_s^\nu \mathbf{s} \| j \rangle \, (a_j^\dagger \times \tilde{a}_{j'})^{(1)} \right\}. \quad (8)$$

The empirical g factors for the neutron and proton bosons, $g_\nu^B = 0\,\mu_N$ and $g_\pi^B = 1.0\,\mu_N$, respectively, are adopted. For the neutron g factors, the standard Schmidt values $g_l^\nu = 0\,\mu_N$ and $g_s^\nu = -3.82\,\mu_N$ are used, with g_s quenched by 30% with respect to the free value.

In Table IV we list the calculated $B(E2)$ and $B(M1)$ transition rates, the electric quadrupole $Q(I)$ and magnetic dipole $\mu(I)$ moments for the odd-A nuclei ^{95,97,99,101}Zr, for which data are available. Only the quadrupole and magnetic moments for the ground state are known for ^{95}Zr. The calculated $Q(5/2_1^+)$ is rather small in magnitude. It is opposite in sign to the experimental value, which is, however, also relatively small in magnitude. The sign of the magnetic moment of ^{95}Zr has not been identified experimentally, but it is likely to be negative from the present calculation. For the ^{97}Zr, all the calculated experimental transition strengths and moments are in a good agreement with the data.

The $B(E2; 7/2_1^+ \to 3/2_1^+)$ transition rate in ^{99}Zr is experimentally suggested to be rather weak [15], similar to the neighboring isotope ^{97}Zr. The predicted $E2$ strength for this transition is a bit larger, but is in the same order of magnitude as the experimental one. The experimental $B(E2; 7/2_2^+ \to 3/2_2^+)$ transition rate of 46 ± 12 W.u. is considerably underestimated by the calculation. As seen in Fig. 6, both the $7/2_2^+$ and $3/2_2^+$ states are in the same band in our calculation. This band is dominated by the $\Delta I = 1$ $E2$ systematics, and the $\Delta I = 2$ $E2$ transitions within the band are much weaker. The phenomenological IBFM calculation performed in Ref. [14] has also underestimated the measured value of this transition strength by a factor of five. In the present calculation the $B(E2)$ values for the negative-parity states in ^{99}Zr are also by a factor of five to six lower than the experimental ones [15]. Nevertheless, the majority of the $B(M1)$ values, as well as the magnetic moments for the low-lying positive-parity states, both the sign and magnitude, are nicely reproduced.

One notices that the electromagnetic properties for ^{101}Zr are, overall, reasonably reproduced. The exceptions are perhaps the $B(E2; 7/2_1^+ \to 3/2_1^+)$ rate, and few small magnetic moments that are obtained with the wrong sign.

V. SIGNATURES OF QUANTUM SHAPE-PHASE TRANSITION

As a signature of quantum phase transition, we consider quadrupole shape invariants [52] computed using the IBM-2

TABLE IV. Calculated and experimental $B(E2)$ and $B(M1)$ transition rates (in Weisskopf units), and quadrupole $Q(I)$ (in units of eb) and magnetic $\mu(I)$ (in units of μ_N) moments for the odd-A nuclei ^{95,97,99,101}Zr. The experimental values are from Refs. [14,15,48,51].

		Theory	Experiment
^{95}Zr	$Q(5/2_1^+)$	−0.021	+0.22(2)
	$\mu(5/2_1^+)$	−1.33	1.13(2)
^{97}Zr	$B(E2;5/2_1^+ \to 1/2_1^+)$	6.2	>0.30
	$B(E2;7/2_1^+ \to 3/2_1^+)$	8.8	1.55(5)
	$B(E2;11/2_1^- \to 7/2_1^-)$	0.15	0.25(6)
	$\mu(1/2_1^+)$	−0.33	−0.937(5)
	$\mu(7/2_1^+)$	+2.54	+1.37(14)
^{99}Zr	$B(E2;7/2_1^+ \to 3/2_1^+)$	9.9	1.16(3)
	$B(E2;7/2_2^+ \to 3/2_2^+)$	2.9	46(12)
	$B(E2;7/2_1^- \to 3/2_1^-)$	0.24	2.1×10^2(7)
	$B(E2;11/2_1^- \to 7/2_1^-)$	16	99(6)
	$B(E2;15/2_1^- \to 11/2_1^-)$	12	60(11)
	$B(E2;19/2_1^- \to 15/2_1^-)$	8.6	66(9)
	$B(M1;3/2_1^+ \to 1/2_1^+)$	0.0057	0.0102(3)
	$B(M1;5/2_1^+ \to 3/2_1^+)$	0.074	0.042(21)
	$B(M1;5/2_1^+ \to 3/2_2^+)$	0.0040	0.0047(20)
	$B(M1;7/2_2^+ \to 5/2_1^+)$	0.0098	0.032(10)
	$B(M1;5/2_1^- \to 3/2_1^-)$	0.0063	0.015(9)
	$\mu(1/2_1^+)$	−0.48	−0.930(4)
	$\mu(3/2_1^+)$	+0.75	+0.42(6)
	$\mu(7/2_1^+)$	+1.21	±2.31(14)
^{101}Zr	$B(E2;5/2_1^+ \to 3/2_1^+)$	69	$3.E + 2_3^4$
	$B(E2;7/2_1^+ \to 3/2_1^+)$	0.00061	$>1.3 \times 10^2$
	$B(E2;7/2_1^- \to 5/2_1^-)$	102	$4.E + 2(5)$
	$B(M1;5/2_1^+ \to 3/2_1^+)$	0.017	0.036(13)
	$B(M1;7/2_1^+ \to 5/2_1^+)$	0.16	>0.091
	$B(M1;7/2_1^- \to 5/2_1^-)$	0.15	0.033
	$Q(3/2_1^+)$	+0.70	+0.81(6)
	$\mu(3/2_1^+)$	−0.09	−0.272(1)
	$\mu(5/2_1^+)$	−0.51	+0.117(65)
	$\mu(7/2_1^+)$	−0.13	$< +0.59(50)$
	$\mu(5/2_1^-)$	−1.33	−0.50(23)
	$\mu(7/2_1^-)$	−1.15	−0.14(11)

and IBFM-2 wave functions. The relevant quadrupole shape invariants for a given IBM-2/IBFM-2 state $|\alpha I\rangle$, where a label α distinguishes states with the same spin I, are defined as [53]

$$q_2 = \langle \alpha I | \left(\hat{Q} \cdot \hat{Q}\right) | \alpha I \rangle , \tag{9}$$

$$q_3 = -\sqrt{\frac{35}{2}} \langle \alpha I | [\hat{Q}\hat{Q}\hat{Q}]^{(0)} | \alpha I \rangle , \tag{10}$$

$$q_4 = \langle \alpha I | (\hat{Q} \cdot \hat{Q})(\hat{Q} \cdot \hat{Q}) | \alpha I \rangle , \tag{11}$$

$$q_6 = \frac{35}{2} \langle \alpha I | [\hat{Q}\hat{Q}\hat{Q}]^{(0)} [\hat{Q}\hat{Q}\hat{Q}]^{(0)} | \alpha I \rangle , \tag{12}$$

where $[\hat{Q}\hat{Q}\hat{Q}]^{(0)} = [[\hat{Q} \times \hat{Q}]^{(2)} \times \hat{Q}]^{(0)}$, and $\hat{Q}$ is the corresponding $E2$ transition operator. The following dimensionless parameters read: $K_n = q_n / q_2^{n/2}$ with $n = 3, 4$, and 6 and provide the link to the usual deformation parameters that

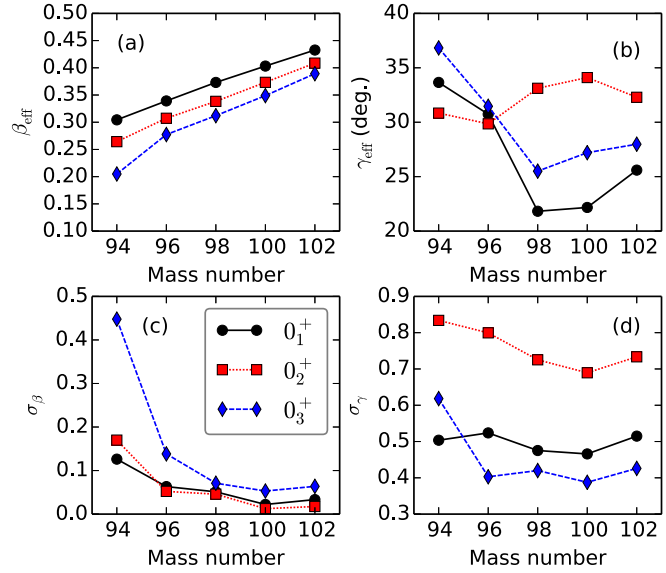

FIG. 9. The effective quadrupole deformation parameters $\beta_{\rm eff}$ (a) and $\gamma_{\rm eff}$ (b), and the fluctuations σ_β (c) and σ_γ (d), calculated for the lowest three 0^+ states of the even-even Zr nuclei.

characterize the shape of a nucleus:

$$K_3 = \frac{\langle \beta^3 \cos 3\gamma \rangle}{\langle \beta^2 \rangle^{3/2}} \equiv \cos 3\gamma_{\rm eff}, \tag{13}$$

$$K_4 = \frac{\langle \beta^4 \rangle}{\langle \beta^2 \rangle^2}, \tag{14}$$

$$K_6 = \frac{\langle \beta^6 \cos^2 3\gamma \rangle}{\langle \beta^2 \rangle^3}. \tag{15}$$

The effective quadrupole deformation parameters read

$$\beta_{\rm eff} = \sqrt{\langle \beta^2 \rangle} = \frac{4\pi}{3eZR^2} \sqrt{q_2}, \tag{16}$$

$$\gamma_{\rm eff} = \frac{1}{3} \arccos K_3, \tag{17}$$

and the corresponding fluctuations of β and $\cos 3\gamma$ can be computed from

$$\sigma_\beta = \frac{\langle \beta^4 \rangle - \langle \beta^2 \rangle^2}{\langle \beta^2 \rangle^2} = K_4 - 1, \tag{18}$$

$$\sigma_\gamma = \frac{\langle \beta^6 \cos^2 3\gamma \rangle - \langle \beta^3 \cos 3\gamma \rangle^2}{\langle \beta^2 \rangle^3} = K_6 - K_3^2. \tag{19}$$

Note that $R = 1.2A^{1/3}$ fm in Eq. (16).

In Figs. 9 and 10 we display $\beta_{\rm eff}$, $\gamma_{\rm eff}$, σ_β, and σ_γ for the even-even and odd-A Zr nuclei, respectively. The signature of a quantum phase transition can be identified as an abrupt change of an order parameter for a particular value of the control parameter. In the present case, in which we consider geometric shape transitions along a chain of isotopes, the neutron number plays the role of the control parameter, while shape invariants or effective (state-dependent) deformations can be considered as order parameters. The quantities defined in Eqs. (16) to (19), that is, the effective deformations and

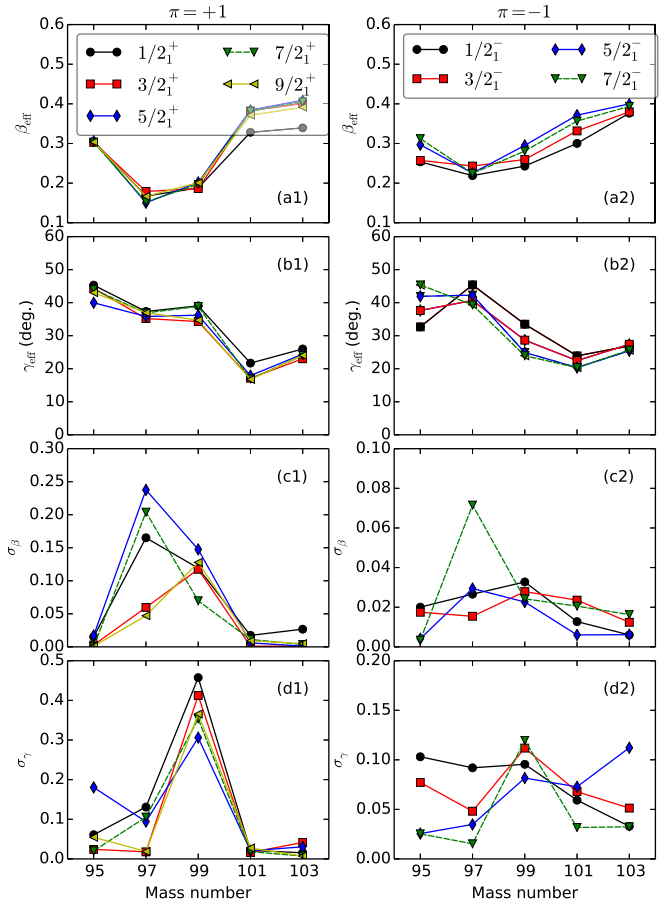

FIG. 10. Same as in the caption to Fig. 9, but for several low-spin yrast states with positive (left column) and negative (right column) parity in the odd-*A* Zr isotopes.

corresponding fluctuations for the lowest-lying states, display discontinuities close to the transitional nucleus ^{98}Zr, at which even-even systems undergo a phase transition. For the even-even isotopes, in Fig. 9, the effective deformations $\beta_{\rm eff}$ of the lowest three 0^+ states increase smoothly with the neutron number and, as a consequence, the fluctuation σ_β does not change much in the vicinity of ^{98}Zr. The particularly large σ_β at ^{94}Zr indicates significant shape mixing. The effective γ deformation, however, exhibits a more pronounced change in the transition from ^{96}Zr to ^{98}Zr for all three 0^+ states. We note, in particular, the large fluctuations in γ for the second 0^+ state.

As shown in Fig. 10 for the odd-*A* Zr nuclei, the effective deformations and corresponding fluctuations of the lowest positive- and negative-parity states exhibit discontinuities characteristic of a shape-phase transition at ^{99}Zr. It is interesting to note that the sudden changes appear to be more pronounced than in the even-even neighbors. A similar effect has been found in the analysis of the microscopic signatures of nuclear ground-state shape-phase transitions in odd-mass Eu isotopes [54] and attributed to a shape polarization effect of the unpaired nucleon. In the present case the strongest signature of a shape-phase transition is provided by the effective deformations and their fluctuations for the lowest positive-parity states. Pronounced discontinuities appear between ^{99}Zr and ^{101}Zr, and their microscopic origin can be clearly identified in the composition of the IBFM-2 wave functions shown in Fig. 8. We note that the enhancement of a shape-phase transition in the presence of an unpaired nucleon has also been explored using a more phenomenological IBFM approach [55].

VI. SUMMARY

Spectroscopic properties relevant for the characterization of shape-phase transitions in even-even and odd-*A* neutron-rich Zr isotopes have been investigated using the microscopic framework of nuclear DFT. Deformation constrained SCMF calculations have been performed with the relativistic Hartree-Bogoliubov method based on the universal energy density functional DD-PC1 and a separable pairing interaction. The triaxial (β, γ) deformation energy surfaces obtained from the SCMF calculations for the even-even $^{94-102}$Zr isotopes predict a very interesting nuclear structure evolution: Shallow triaxial deformations in ^{94}Zr, a γ-unstable potential in ^{96}Zr, coexistence of a shallow oblate and strongly deformed prolate minimum in ^{98}Zr, and the occurrence of γ softness in ^{100,102}Zr. These SCMF results corroborate the conclusions of recent experimental studies.

The excitation spectra of the even-even Zr nuclei have been computed by mapping the SCMF deformation energy surfaces onto the expectation value of the IBM-2 Hamiltonian in the boson condensate state. A phase-transitional behavior of the low-lying excitation spectra, that occurs between ^{96}Zr and ^{100}Zr, is qualitatively reproduced. The excitation energies of the low-lying second 0^+ in ^{98,100}Zr are, however, considerably overestimated in the present calculation. These low-lying 0^+ excitation energies have previously been explained by effects such as shape coexistence related to intruder configurations or pairing vibrations, both of which are outside the configuration space of the present IBM framework.

Spectroscopic properties of the odd-*A* Zr nuclei are computed by means of the particle-core coupling of the IBFM. The SCMF calculations provide a microscopic input for the construction of the basic parts of the IBFM Hamiltonian. The calculated low-energy spectra of the odd-*A* Zr isotopes exhibit interesting structural evolution close to the neutron number $N = 59$, and are in very good agreement with the experimental results. In ^{95,97}Zr, both the positive- and negative-parity spectra correspond to a weak coupling of a vibrational even-even core to the odd particle (neutron in this case). For ^{101,103}Zr, bands typical of the odd nucleon strongly coupled to a well-deformed even-even core appear as yrast structures. The low-energy spectra for the transitional nucleus ^{99}Zr can be characterized by the coexistence of $\Delta I = 1$ and $\Delta I = 2$ positive-parity bands. The calculated quadrupole shape invariants provide a signature of a shape-phase transition. The interesting result is that, for the odd-*A* Zr isotopes, the effective deformations β and γ, and their fluctuations exhibit more pronounced discontinuities at the point of shape-phase transition when compared to their even-even neighbors.

Taking into account that a microscopic SCMF calculation based on a universal EDF completely determines the

even-even core Hamiltonian and most of the IBFM Hamiltonian, and that only a few adjustable parameters specify the fermion-boson terms, this approach holds promise for exploring simultaneously even-even and odd-mass neutron-rich nuclei in this challenging region of the nuclear chart. A prospect for future studies is to improve the description of the even-even Zr nuclei, especially the low-lying excited 0^+ states. In this respect, a configuration-mixing IBM calculation based on the Gogny HFB has already been reported for the even-even Zr isotopes [10]. It will be interesting to develop a formalism that incorporates these additional effects consistently both for even-even and odd-*A* systems.

ACKNOWLEDGMENTS

This work has been supported by the Tenure Track Pilot Programme of the Croatian Science Foundation and the École Polytechnique Fédérale de Lausanne, and the Project TTP-2018-07-3554 Exotic Nuclear Structure and Dynamics, with funds of the Croatian-Swiss Research Programme. It has also been supported in part by the QuantiXLie Centre of Excellence, a project cofinanced by the Croatian Government and European Union through the European Regional Development Fund—the Competitiveness and Cohesion Operational Programme (KK.01.1.1.01).

[1] P. Cejnar, J. Jolie, and R. F. Casten, Rev. Mod. Phys. **82**, 2155 (2010).
[2] K. Heyde and J. L. Wood, Rev. Mod. Phys. **83**, 1467 (2011).
[3] D. A. Sazonov, E. A. Kolganova, T. M. Shneidman, R. V. Jolos, N. Pietralla, and W. Witt, Phys. Rev. C **99**, 031304(R) (2019).
[4] P. Singh, W. Korten, T. W. Hagen, A. Görgen, L. Grente, M.-D. Salsac, F. Farget, E. Clément, G. de France, T. Braunroth *et al.*, Phys. Rev. Lett. **121**, 192501 (2018).
[5] W. Witt, V. Werner, N. Pietralla, M. Albers, A. D. Ayangeakaa, B. Bucher, M. P. Carpenter, D. Cline, H. M. David, A. Hayes *et al.*, Phys. Rev. C **98**, 041302(R) (2018).
[6] C. Kremer, S. Aslanidou, S. Bassauer, M. Hilcker, A. Krugmann, P. von Neumann-Cosel, T. Otsuka, N. Pietralla, V. Y. Ponomarev, N. Shimizu *et al.*, Phys. Rev. Lett. **117**, 172503 (2016).
[7] S. Ansari, J.-M. Régis, J. Jolie, N. Saed-Samii, N. Warr, W. Korten, M. Zielińska, M.-D. Salsac, A. Blanc, M. Jentschel *et al.*, Phys. Rev. C **96**, 054323 (2017).
[8] W. Urban, T. Rzaca-Urban, J. Wiśniewski, A. G. Smith, G. S. Simpson, and I. Ahmad, Phys. Rev. C **100**, 014319 (2019).
[9] T. Togashi, Y. Tsunoda, T. Otsuka, and N. Shimizu, Phys. Rev. Lett. **117**, 172502 (2016).
[10] K. Nomura, R. Rodríguez-Guzmán, and L. M. Robledo, Phys. Rev. C **94**, 044314 (2016).
[11] J. E. García-Ramos and K. Heyde, Phys. Rev. C **100**, 044315 (2019).
[12] N. Gavrielov, A. Leviatan, and F. Iachello, Phys. Rev. C **99**, 064324 (2019).
[13] T. Rzaca-Urban, W. Urban, M. Czerwiński, J. Wiśniewski, A. Blanc, H. Faust, M. Jentschel, P. Mutti, U. Köster, T. Soldner *et al.*, Phys. Rev. C **98**, 064315 (2018).
[14] P. Spagnoletti, G. Simpson, S. Kisyov, D. Bucurescu, J.-M. Régis, N. Saed-Samii, A. Blanc, M. Jentschel, U. Köster, P. Mutti *et al.*, Phys. Rev. C **100**, 014311 (2019).
[15] F. Boulay, G. S. Simpson, Y. Ichikawa, S. Kisyov, D. Bucurescu, A. Takamine, D. S. Ahn, K. Asahi, H. Baba, D. L. Balabanski *et al.*, Phys. Rev. Lett. **124**, 112501 (2020).
[16] A. Bohr and B. M. Mottelsson, *Nuclear Structure* (Benjamin, New York, 1975), Vol. 2.
[17] K. Nomura, T. Nikšić, and D. Vretenar, Phys. Rev. C **93**, 054305 (2016).
[18] M. Bender, P.-H. Heenen, and P.-G. Reinhard, Rev. Mod. Phys. **75**, 121 (2003).
[19] D. Vretenar, A. Afanasjev, G. Lalazissis, and P. Ring, Phys. Rep. **409**, 101 (2005).
[20] L. M. Robledo, T. R. Rodríguez, and R. R. Rodríguez-Guzmán, J. Phys. G: Nucl. Part. Phys. **46**, 013001 (2019).
[21] F. Iachello and A. Arima, *The Interacting Boson Model* (Cambridge University Press, Cambridge, 1987).
[22] F. Iachello and P. Van Isacker, *The Interacting Boson-Fermion Model* (Cambridge University Press, Cambridge, 1991).
[23] K. Nomura, T. Nikšić, and D. Vretenar, Phys. Rev. C **94**, 064310 (2016).
[24] K. Nomura, T. Nikšić, and D. Vretenar, Phys. Rev. C **96**, 014304 (2017).
[25] K. Nomura, T. Nikšić, and D. Vretenar, Phys. Rev. C **97**, 024317 (2018).
[26] K. Nomura, R. Rodríguez-Guzmán, and L. M. Robledo, Phys. Rev. C **101**, 014306 (2020).
[27] K. Nomura, R. Rodríguez-Guzmán, and L. M. Robledo, Phys. Rev. C **101**, 024311 (2020).
[28] K. Nomura, R. Rodríguez-Guzmán, and L. M. Robledo, Phys. Rev. C **101**, 044318 (2020).
[29] T. Nikšić, D. Vretenar, and P. Ring, Phys. Rev. C **78**, 034318 (2008).
[30] Y. Tian, Z. Y. Ma, and P. Ring, Phys. Lett. B **676**, 44 (2009).
[31] K. Nomura, D. Vretenar, T. Nikšić, and B.-N. Lu, Phys. Rev. C **89**, 024312 (2014).
[32] K. Nomura, N. Shimizu, D. Vretenar, T. Nikšić, and T. Otsuka, Phys. Rev. Lett. **108**, 132501 (2012).
[33] T. Nikšić, P. Marević, and D. Vretenar, Phys. Rev. C **89**, 044325 (2014).
[34] Z. P. Li, T. Nikšić, and D. Vretenar, J. Phys. G: Nucl. Part. Phys. **43**, 024005 (2016).
[35] P. Marević, J.-P. Ebran, E. Khan, T. Nikšić, and D. Vretenar, Phys. Rev. C **97**, 024334 (2018).
[36] J. Zhao, B.-N. Lu, T. Nikšić, D. Vretenar, and S.-G. Zhou, Phys. Rev. C **93**, 044315 (2016).
[37] J. Zhao, J. Xiang, Z.-P. Li, T. Nikšić, D. Vretenar, and S.-G. Zhou, Phys. Rev. C **99**, 054613 (2019).
[38] J. F. Berger, M. Girod, and D. Gogny, Nucl. Phys. A **428**, 23 (1984).
[39] http://www-phynu.cea.fr/science_en_ligne/carte_potentiels_microscopiques/carte_potentiel_nucleaire_eng.htm.
[40] S. Goriely, S. Hilaire, M. Girod, and S. Péru, Phys. Rev. Lett. **102**, 242501 (2009).

[41] P. Ring and P. Schuck, *The Nuclear Many-Body Problem* (Springer-Verlag, Berlin, 1980).
[42] K. Nomura, N. Shimizu, and T. Otsuka, Phys. Rev. Lett. **101**, 142501 (2008).
[43] T. Otsuka, A. Arima, and F. Iachello, Nucl. Phys. A **309**, 1 (1978).
[44] P. D. Duval and B. R. Barrett, Phys. Lett. B **100**, 223 (1981).
[45] K. Nomura, T. Otsuka, N. Shimizu, and L. Guo, Phys. Rev. C **83**, 041302(R) (2011).
[46] A. Leviatan and D. Shapira, Phys. Rev. C **93**, 051302(R) (2016).
[47] N. Yoshida, H. Sagawa, and T. Otsuka, Nucl. Phys. A **567**, 17 (1994).
[48] Brookhaven National Nuclear Data Center, http://www.nndc.bnl.gov.
[49] M. Matejska-Minda, B. Fornal, R. Broda, M. P. Carpenter, R. V. F. Janssens, W. Królas, T. Lauritsen, P. F. Mantica, K. Mazurek, T. Pawłat *et al.*, Phys. Rev. C **80**, 017302 (2009).
[50] R. Orlandi, A. G. Smith, D. Patel, G. S. Simpson, R. M. Wall, J. F. Smith, O. J. Onakanmi, I. Ahmad, J. P. Greene, M. P. Carpenter *et al.*, Phys. Rev. C **73**, 054310 (2006).
[51] N. Stone, At. Data Nucl. Data Tables **90**, 75 (2005).
[52] D. Cline, Annu. Rev. Nucl. Part. Sci. **36**, 683 (1986).
[53] V. Werner, N. Pietralla, P. von Brentano, R. F. Casten, and R. V. Jolos, Phys. Rev. C **61**, 021301(R) (2000).
[54] S. Quan, Z. P. Li, D. Vretenar, and J. Meng, Phys. Rev. C **97**, 031301(R) (2018).
[55] D. Petrellis, A. Leviatan, and F. Iachello, Ann. Phys. (NY) **326**, 926 (2011).